

---

**ORIGINAL ARTICLE****Journal Section**

# Quantification of the seasonal hillslope water storage that does not drive streamflow

David N. Dralle<sup>1</sup> | W. Jesse Hahm<sup>1</sup> | Daniella M. Rempe<sup>2</sup> | Nathaniel J. Karst<sup>3</sup> | Sally E. Thompson<sup>4</sup> | William E. Dietrich<sup>1</sup>

<sup>1</sup>Department of Earth and Planetary Science, University of California Berkeley, Berkeley CA, USA

<sup>2</sup>Jackson School of Geosciences, Department of Geological Science, University of Texas, Austin, TX USA

<sup>3</sup>Mathematics and Science Division, Babson College, Wellesley MA, USA

<sup>4</sup>Department of Civil and Environmental Engineering, University of California Berkeley, Berkeley CA, USA

**Correspondence**

David N. Dralle, Department of Earth and Planetary Science, University of California Berkeley, Berkeley CA, USA  
Email: dralle@berkeley.edu

**Funding information**

National Science Foundation CZP EAR-1331940 for the Eel River Critical Zone Observatory; University of California Natural Reserve System Mildred E. Mathias Graduate Student Research Grant

The relationship between seasonal catchment water storage and discharge is typically non-unique as a result of water storage that is not directly hydraulically connected to streams. These hydraulically disconnected water volumes are often ecologically and hydrologically important, but cannot be explicitly estimated using current storage-discharge techniques. Here, we propose that discharge is explicitly sensitive to changes in only some fraction of seasonally dynamic storage that we call “direct storage”, while the remaining storage (“indirect storage”) varies without directly influencing discharge. We use a coupled mass balance and storage-discharge function approach to partition seasonally dynamic storage between these two pools at two neighboring field sites in the Northern California Coast Ranges. We find that indirect storage constitutes the vast majority of dynamic catchment storage, even at the wettest times of the year. Indirect storage exhibits lower variability over the course of the wet season (and in successive winter periods), than does direct storage. Predicted indirect storage volumes and dynamics match field observations at both field sites. Comparison of the two field sites reveals that indirect storage volumes can occur as unsaturated storage held under tension in soils and weathered bedrock, and as near-surface

saturated storage that remains on hillslopes (and is eventually evapotranspired). Indirect storage volumes (including moisture in the weathered bedrock) may support plant transpiration, and our method indicates this important water source could be quantified from precipitation and stream discharge records.

#### KEY WORDS

dynamic storage, water balance, recession analysis, critical zone, unsaturated moisture, saturated moisture

## 1 | MOTIVATION

Hydrologists have long sought physically-based formulations of discharge behavior that are sufficiently complex to describe the diverse behaviors of watersheds without including unnecessary degrees of freedom that challenge model uniqueness (e.g. Dupuit, 1863; Horton, 1936; Brutsaert and Nieber, 1977; Rodríguez-Iturbe and Valdés, 1979; Beven, 1989). At catchment scales, this pursuit is arguably most simply manifested in storage-discharge functions: continuous, monotonic functions of catchment or hillslope water storage that return a corresponding value of stream discharge (Coutagne, 1948; Hall, 1968; Sloan, 2000; Kirchner, 2009). The relationship between catchment water storage and release is in some sense a reflection of the physical structure and organization of the subsurface components of the critical zone (CZ) (Creutzfeldt et al., 2013; Buttle, 2016), the hydrologically permeable mantle of weathered material from fresh bedrock at depth up through the overlying vegetation canopy. Because of difficulties associated with observing subsurface CZ attributes (Holbrook et al., 2014; Riebe et al., 2016; Grant and Dietrich, 2017), an appealing feature of storage-discharge relationships is their ease of inversion, which can allow inference of difficult-to-observe critical zone storage dynamics from observations of discharge. In many catchments, however, inversion is challenged by the observation that the relationship between storage and discharge is non-unique, suggesting the presence of potentially large volumes of catchment storage that can vary seasonally, but do not directly influence discharge generation (Brauer et al., 2013; Staudinger et al., 2017). Storage of this type has been termed ‘hydraulically decoupled’ (Rieger and Tourian, 2014), and may include snow, ice, ponds, tension-held unsaturated water (Krier et al., 2012), water on vegetation, or laterally disconnected groundwater (Spence et al., 2009; van Meerveld and McDonnell, 2006; Nippgen et al., 2015).

Hydraulic decoupling of certain catchment storage elements from streams is central to our present understanding of watershed discharge generation. For example, the often-observed threshold response of discharge to precipitation events can in some cases be attributed to hysteretic water transmission to streams, so that certain catchment storage must be filled before significant discharge volumes can be generated (Spence et al., 2009; Sayama et al., 2011; Salve et al., 2012; Hahm et al., 2017a; Rempe, 2016). These storage elements could be unsaturated and drain at a ‘field capacity’ to aquifers that feed streams (e.g. Botter et al., 2007; Torres et al., 1998); or saturated and drain as groundwater flow to streams.

Associated with nonlinear, hysteretic storage-discharge mechanisms are time-lags in the transfer of mass or information through a watershed, suggesting that the volume and physical attributes (for example, saturated versus unsaturated) of decoupled storage have important implications for understanding catchment transport timescales, hydraulic response to external fluxes, and the sensitivity of evapotranspiration to climate variations (e.g. Torres et al.,

1998; Tani, 2008; Rieger and Tourian, 2014; Nippgen et al., 2016). Correspondingly, conceptual hydrologic models often feature decoupled storage elements (e.g. Lehmann et al., 2007; Botter et al., 2009; Birkel et al., 2011), whose process representations are strong determinants of catchment discharge response and the emergent, hysteretic features of modeled storage-discharge relationships (Fovet et al., 2015). Thus, estimating the volumes and temporal dynamics of hydraulically decoupled catchment storage could provide important new insights into catchment processes and improve hydrological modeling frameworks.

Here, we pair mass balance with a storage-discharge function to partition seasonal volumes of catchment water storage between hydraulically coupled and decoupled subsurface storage elements – termed *direct storage* and *indirect storage*, respectively. Applying the method at two intensively-monitored experimental watersheds in the Franciscan Formation complex within the Coast Ranges of Northern California, we find that the dynamic catchment water storage is primarily indirect, even during the wettest times of year. While volumes of direct storage vary significantly throughout the wet season, indirect storage volumes remain relatively constant. We evaluate the method's accuracy using *in situ* measurements of catchment storage volumes. At both sites, the method identifies storage volume differences that are consistent with critical zone water storage capacity. The method performs adequately at both field sites even though critical zone structure is deep at one site and shallow at the other, which leads to large differences in the physical interpretation of indirect storage volumes.

## 2 | METHODS

Mass balance methods and the concept of 'dynamic storage' are often used to describe catchment-scale storage behavior. Dynamic storage is defined as the volume of catchment storage that exceeds some fixed reference state, such as the storage at the end of the dry season or water year. It differs from the absolute volume of water storage in a catchment, which cannot typically be determined from a water balance due to measurement difficulties and an ill-defined lower boundary condition. Dynamic storage has been used to compare storage and transport properties between catchments (McNamara et al., 2011; Buttle, 2016), and as a key variable in lumped hydrologic models (e.g. Botter et al., 2009). It has been estimated using remotely sensed and gravimetric techniques (Creutzfeldt et al., 2013; Rieger and Tourian, 2014), mass-balance and recession-based methods (e.g. Sayama et al., 2011; Kirchner, 2009), and hydrologic models (e.g. Birkel et al., 2011).

Here we adopt a dynamic storage description similar to that proposed by Sayama et al. (2011): *Total dynamic storage* ( $S_T$ ) is the increase in total storage inferred from running a catchment-wide mass balance between an initial time ( $t = 0$ ), when total catchment storage can be assumed to have reached an effective minimum value ( $S(0) = S_{min}$ ), and time  $t$ , such that,

$$S_T(t) \approx S(t) - S_{min} = \int_0^t (P - Q - ET) d\tau. \quad (1)$$

Here,  $P$  [L/T] is spatially averaged, effective precipitation (precipitation minus interception),  $ET$  [L/T] is catchment evapotranspiration (not including evaporated interception water),  $Q$  [L/T] is catchment discharge,  $S_{min}$  is the minimum value of total catchment storage (typically unknown), and  $\tau$  is a dummy integration variable. Equation 1 assumes inter-basin flow is negligible. To extend Sayama et al. (2011), we propose that total dynamic storage can be partitioned into two distinct volumes:

$$S_T = S_d + S_i \quad (2)$$

defined as:

- Direct storage ( $S_d$  [L]) is the portion of total dynamic storage that drives discharge generation. We assume that the hydraulic gradients driving discharge generation respond monotonically to direct storage, such that the relationship between discharge ( $Q$  [L/T]) and direct storage is fully specified by an invertible storage-discharge function,  $Q = f(S_d)$ . The function  $f$  maps each value of direct storage to a unique value of discharge.
- Indirect storage ( $S_i$  [L]) is the volume of dynamic storage in the catchment that remains after accounting for direct storage ( $S_i = S_T - S_d$ ). By definition, catchment discharge is not explicitly sensitive to this storage volume. This is not to say that the behavior of  $Q$  is unaffected by  $S_i$ , discharge response to a given precipitation event may be larger or smaller (or more or less prompt) depending on the value  $S_i$ , and yet, knowledge of  $S_i$  is insufficient to determine a unique value for  $Q$ .

We introduce the conceptual terms indirect and direct storage because the former has never been explicitly calculated from recession limb analysis, and the latter is easily confused with similarly defined terms from other studies. For example, Sayama et al. (2011) calculate a seasonal (time-dependent) 'dynamic storage' for two Northern California watersheds, which is equivalent to our 'total dynamic storage' (although Sayama et al. (2011) assume ET is negligible in the water balance). This is distinct from the 'dynamic storage' introduced by Kirchner (2009) and discussed by Staudinger et al. (2017), which is computed from a discharge recession analysis and equal to the maximum range of our 'direct storage'. Similarly, Staudinger et al. (2017) defined 'extended dynamic storage', which is equivalent to the maximum range of our 'total dynamic storage'. The closest definition from Staudinger et al. (2017) to indirect storage would be the difference between their 'extended dynamic storage' and 'dynamic storage'. However, this is not entirely correct because the variables in Staudinger-2017 are computed as a maximum range of storages, whereas 'direct' and 'indirect' storage are time varying quantities. We propose that it is more appropriate to introduce new terminology rather than try to force our concepts into existing frameworks that are either ambiguous (e.g. the difference in the definitions of 'dynamic storage' between Staudinger-2017 and Sayama-2011), or unable to describe the direct and indirect storage as we have defined them.

## 2.1 | A new approach to compute indirect storage

Beginning with Equations 1 and 2, and assuming that total storage is equal to its minimum value ( $S(t) = S_{min}$  at  $t = 0$ ), the whole catchment water balance can be written as:

$$S_T(t) = S_i(t) + S_d(t) = \int_0^{S_d(t)} dS_d + \int_0^{S_i(t)} dS_i = \int_0^t (P - Q - ET) d\tau, \quad (3)$$

where  $S_T(0) = 0$  because total storage is at a minimum, implying that  $S_d$  and  $S_i$  are also zero at  $t = 0$ . In general, catchment evapotranspiration is difficult to predict or observe, and likely depends on climatic conditions and the partitioning of total dynamic storage between  $S_d$  and  $S_i$ . However, under circumstances where  $P$  and  $ET$  are negligible ( $Q \gg P, ET$ ), and assuming any transfers of water between the direct and indirect pools (represented by the flux  $R$

[L/T] in Figure 1) are small relative to  $Q$  ( $Q \gg |R|$ ), changes in direct storage are determined primarily by  $Q$ , so that:

$$\frac{dS_d}{dt} \approx -Q. \quad (4)$$

This relationship can be used with the chain rule to estimate the catchment sensitivity function,  $g(Q)$  (Kirchner, 2009):

$$g(Q) = \frac{dQ}{dS_d} \quad (5a)$$

$$= \frac{dQ/dt}{dS_d/dt} \quad (5b)$$

$$\approx -\left. \frac{dQ/dt}{Q} \right|_{Q \gg P, ET, R}. \quad (5c)$$

The sensitivity function  $g(Q) = dQ/dS_d$  is not a statement of mass balance; it represents the mathematical sensitivity of  $Q$  to changes in  $S_d$ . Therefore, although  $g(Q)$  can only be estimated by Equation 5c during periods when Equation 4 holds, it can be applied outside of these periods to estimate changes in direct storage using only changes in  $Q$ . Differential changes in  $Q$  can be related to changes in  $S_d$  as:

$$dS_d = \frac{dQ}{g(Q)} \iff S_d(t) = \int_{Q(0)}^{Q(t)} \frac{dQ}{g(Q)}. \quad (6)$$

We substitute Equation 6 into Equation 3 and solve for indirect storage:

$$S_i(t) = \int_0^t (P - Q - ET)d\tau - S_d(t). \quad (7)$$

Estimating Equations 6 and 7 demonstrate that, with a set of reasonable assumptions, knowledge of the catchment storage-discharge relationship can be paired with a simple water balance to infer two distinct volumes that constitute total dynamic catchment storage: that storage whose magnitude directly influences discharge ( $S_d$ ), and that which does not ( $S_i$ ).

## 2.2 | Case studies

We rely on stream discharge records and observations of subsurface moisture and ground water dynamics to estimate and interpret direct and indirect dynamic storage in two seasonally dry, Northern California watersheds: Elder Creek (16.9 km<sup>2</sup>), and Dry Creek (3.5 km<sup>2</sup>) (see regional map in Figure 2). Both sites are part of the Eel River Critical Zone Observatory (ERCZO) and have been subject to intensive hillslope monitoring (Salve et al., 2012; Link et al., 2014; Oshun et al., 2016; Kim et al., 2014; Hahm et al., 2017a; Lovill et al., 2015; Rempe, 2016). The regional Mediterranean-type climate here produces warm, dry summers followed by cool, wet winters (Peel et al., 2007). Elder Creek receives approximately 2000 mm of annual precipitation, and Dry Creek receives approximately 1800 mm (PRISM, 2015), most of which falls between November and March. Our sites lie within the Franciscan Formation, an exhumed subduction complex that is locally comprised of three coast-parallel (roughly north-south) belts (see Figure 2 in the present work

Blake Jr. and Jones, 1974). The Elder Creek watershed is located in the westernmost Coastal Belt, which is comprised mostly of shale (argillite), with lesser components of sandstone and conglomerate (Jayko et al., 1989; Salve et al., 2012; Lovill et al., 2015). Dry Creek watershed is about 20 km to the southeast and is underlain by the Central Belt, which consists of mélange with an intensely-sheared, primarily argillaceous matrix with coherent blocks of various lithologies, dominated by sandstone (Blake Jr. and Jones, 1974; Lovill et al., 2015). Table 1 summarizes the physiographic and climatic features of the two sites.

Despite the proximity and similar climates of the sites, their contrasting lithologies lead to dramatic differences in depth of weathering and structure of the critical zone, and corresponding large differences in storage dynamics that provide an exceptional opportunity to test the analysis method proposed here. These differences also likely explain the dominance of evergreen forest canopy in Elder Creek and of winter-deciduous oak annual grassland savanna in Dry Creek (Hahm et al., 2017a).

## 2.2.1 | Elder Creek: Hillslope monitoring and stream discharge

Figure 3 shows a shaded relief map of the Elder Creek watershed (inset) and local topography in the vicinity of the intensive monitoring site (noted by well locations). Here some 700 data streams are used to monitor hydrologic dynamics across a 4000 m<sup>2</sup> hillslope (see Rempe (2016) for much more detail), many of which have been reporting for nearly a decade. Extensive fieldwork throughout the Elder Creek watershed shows that the argillite lithology underlying the intensively monitored hillslope (referred to as “Rivendell”) dominates Elder Creek as a whole (Lovill et al., 2015). Discharge monitoring in Elder Creek has been conducted since 1967 by the United States Geological Survey at a gauge (site id 11475560) approximately 200 m upstream from Rivendell.

At Rivendell a thin soil (30 to 75 cm thick) mantles up to 4 meters of saprolite under which lies weathered, fractured bedrock that systematically varies in thickness from approximately 4 meters near the base of hillslopes to upwards of 20 m at the ridge (Salve et al., 2012; Rempe, 2016; Oshun et al., 2016). The base of weathered, fractured bedrock is underlain by fresh, perennially-saturated unweathered bedrock that acts as an aquiclude to meteoric water. This structured critical zone sets up a repeated, annual cycle of water dynamics, revealed by the field monitoring.

At the start of the wet season, incoming autumn rains progressively increase moisture content in the upper layers of soil, saprolite, and fractured weathered rock (Rempe, 2016). After approximately 300 - 600 mm of cumulative seasonal rainfall, the thick unsaturated zone moisture content no longer increases (Salve et al., 2012; Rempe, 2016). Further rainfall likely travels vertically along fractures and recharges a hillslope water table positioned upon the underlying fresh bedrock boundary. At this boundary, water moves laterally through a network of fractures, eventually reaching the stream through seeps and springs (Salve et al., 2012; Lovill et al., 2015; Rempe, 2016).

Once the groundwater receives winter recharge, successive rainstorms raise the water table to various heights with different timing depending on location on the hillslope (Rempe, 2016). The range of water table depths between successive storms can be many meters, and is commonly characterized by a rapid rise and slower fall. At the end of the wet season, water table levels slowly recede, returning to similar, low levels in successive years.

## 2.2.2 | Dry Creek and the monitored hilltop

Figure 4 shows a bare-earth hillshade map of Dry Creek watershed and the intensively monitored site. The Dry Creek watershed is less steep than Elder Creek and much of the landscape experiences some level of earthflow displacement (Roering et al., 2009; Lee et al., 2017; Lovill et al., 2015). The intensively monitored ridge-top site consists of 8 wells and a weather station. Wells are cased with slotted PVC pipe and drilled beyond the depth of unweathered, fresh bedrock,

which is determined by a lack of weathering, increased material strength, and permanent saturation (Hahm et al., 2017a). A stream gauge approximately 1.4 km downstream of the ridge top site was installed by ERCZO researchers in December 2015. The monitored hilltop has been the subject of a detailed ecophysiological study on *Quercus garryana*, the Oregon White Oak, the predominant tree species at the site (Hahm et al., submitted). Here, too Lovill et al. (2015) report fieldwork across the entire watershed and find that the intensely sheared mélange matrix underlying the monitored site is likely representative of the lithology in Dry Creek. About 12% of the Dry Creek watershed is composed of large sandstone blocks embedded in the mélange matrix (Lovill et al., 2015).

The critical zone is shallow in the mélange. The upper 1.5 - 3 m of thin organic soils and clay-rich weathered matrix are underlain by unweathered, perennially saturated mélange (Cloos, 1983), which has low porosity and saturated hydraulic conductivity (Hahm et al., 2017a). These physical properties of the mélange affect the hydrology of Dry Creek. The first rains of the wet season increase unsaturated moisture content in surface soils and weathered parent material without triggering a response from shallow groundwater. By 200 mm of cumulative wet season rainfall, water tables rise to within 20cm of the ground surface in all wells, and discharge to the stream occurs as shallow subsurface flow and saturation overland flow. Field surveys reveal that after a significant rainfall in winter, essentially the entire landscape sheds water as shallow subsurface storm flow and overland flow.

The shallow depth to fresh bedrock and the consequent winter saturation and rapid water delivery to channels leave little storage to sustain summer baseflows, causing Dry Creek to stop flowing typically by the end of May or beginning of June. Despite receiving annual rainfall totals similar to Elder Creek, Dry Creek's small stores of subsurface water are insufficient to support dense forest, and the dominant land cover type is winter-deciduous oak annual grassland savanna (Hahm et al., 2017a, submitted, 2017b). The sandstone blocks suspended in the mélange support patches of mixed broadleaf-needleleaf evergreen forest similar to those found in the Elder Creek on the Coastal Belt (Lovill et al., 2015).

## 2.2.3 | Site data used to calculate direct and indirect storage

### Discharge

We obtain discharge records from the United States Geological Survey Elder Creek gauge near Branscomb, CA (gauge id: 11475560), which sits approximately 200 m upstream from the base of the Rivendell hillslope (Figure 3). At Dry Creek, a rating curve based on 33 discharge measurements has been used to convert the water level recording to continuous discharge (Hahm et al., 2017a).

### Precipitation

We measure local precipitation at each site with a Campbell Scientific Model TB4 tipping bucket rain gauge, and apply a wind-correction factor following the procedure outlined in Yang et al. (1998). Dry Creek precipitation is measured at a ridge-top gauging station located approximately 1.5 km from the catchment centroid, and Elder Creek precipitation is averaged between a gauge located near the watershed outlet and a higher elevation gauge in the headwaters. A third gauging station in the Elder Creek watershed (Campbell Scientific TE525 Tipping Bucket located in a meadow weather station approximately 0.5 km from the Elder Creek watershed) has logged precipitation data since 2008 but exhibits a slight bias in rainfall totals relative to the newer TB4 gauges. We use the TB4 precipitation data to estimate a simple bias correction factor for the longer running gauge, increasing TE525 daily rainfall rates by a constant factor (equal to 1.17) so that precipitation totals match for the period of time over which gauge records overlap.

## Other measurements

Weather stations located on the ridge at Dry Creek (Figure 4) and a meadow near Elder Creek (Figure 3) record air temperature used for calculation of potential evapotranspiration. Measurements of saturated hydraulic conductivity with depth were taken at the Dry Creek site at three ridge-top hillslope locations near wells 506-508 (Figure 4) within predominantly mélange matrix. These measurements were taken using a Guelph permeameter and the single head method detailed in Elrick and Reynolds (1992).

### 2.2.4 | Determination of site storage-discharge relationships

Accurate determination of the catchment sensitivity function,  $g(Q)$ , is central to the subsequent analyses, and relies on satisfaction of Equation 4 ( $ET, P, R \ll Q$ ). To ensure  $ET \ll Q$ , we restrict analysis to the months of November, December, January, February, and March, when rates of catchment evapotranspiration are much less than winter discharge. To avoid confounding effects of precipitation fluxes into direct storage, we discard 24 hours of data immediately following any significant rainfall event (greater than 2mm over 24 hours). We also assume that this restriction is sufficient to exclude periods of time during which large transfers between direct and indirect storage occur.

Following Palmroth et al. (2010), we estimate  $dQ/dt$  using a variable time-step method (Rupp and Selker, 2006), where  $\Delta t$  at time  $t$  is minimal value such that  $\Delta Q = Q(t) - Q(t - \Delta t) > 0.001\bar{Q}$ , and  $\bar{Q}$  is the long-term discharge mean over all available data from the analysis months (Nov - Mar). For each estimated  $dQ/dt \approx \Delta Q/\Delta t$ , we choose a corresponding estimate of  $Q$  equal to the arithmetic mean of all discharge values over the interval  $[t - \Delta t, t]$ . We bin the collection of  $dQ/dt$  from the smallest to largest corresponding values of  $Q$ , so that each bin spans at least 1% of the logarithmic range in  $Q$  (Kirchner, 2009). Because our analysis uses daily discharge values and records are relatively short (only 51 days satisfied the requirements for recession analysis at Dry Creek), we also require a minimum number of seven data points in each bin. Following binning, we use weighted linear regression to fit a quadratic relationship between  $\log(Q)$  and binned values of  $\log(-dQ/dt)$ :

$$\log(-dQ/dt) = p_0 + p_1 \log Q + p_2(\log Q)^2. \quad (8)$$

Regression weights are equal to the reciprocal of the square of the standard error of each binned value of  $\log(-dQ/dt)$ . Figure 5 demonstrates the results of this fitting procedure for Elder Creek and Dry Creek. By subtracting  $\log Q$  from both sides of Equation 8, the catchment sensitivity function can be expressed in terms of the fitted coefficients from Figure 5 ( $p_0$ ,  $p_1$ , and  $p_2$ ):

$$g(Q) = \log\left(-\frac{dQ/dt}{Q}\right) = p_0 + (p_1 - 1)\log Q + p_2(\log Q)^2. \quad (9)$$

### 2.2.5 | Estimating evapotranspiration and effective precipitation

Evapotranspiration is assumed to proceed at the potential rate ( $ET = E_p$ ) during the wet season months when catchments are strongly energy limited. This simplifying assumption is possible due to the Mediterranean climate at our sites. Under water-limited scenarios,  $ET$  would need to be estimated with a model or using remotely-sensed data. We compute  $E_p$  using the Hargreaves equation (Hargreaves and Samani, 1985), in the form of Equation 52 from Allen et al. (1998):

$$E_p = 0.0023 \cdot (T_{mean} + 17.8) \cdot (T_{max} - T_{min})^{0.5} \cdot 0.408 \cdot R_{ext}. \quad (10)$$

$T_{mean}$ ,  $T_{max}$ , and  $T_{min}$  are the daily mean, maximum, and minimum temperatures, respectively, obtained from Eel River Critical Zone Observatory weather station data (Figures 3 and 4). Extra-terrestrial solar radiation ( $R_{ext}$ ) is computed from the site latitude and day of year according to Allen et al. (1998).

We apply a simple interception model, where interception is equal to rainfall on day  $i$  if precipitation on day  $i$  is less than a threshold  $\Delta$ , and equal to  $\Delta$  if rainfall on day  $i$  is greater than  $\Delta$  (Lai et al., 2001). We do not subtract intercepted rainfall from daily  $E_p$ , which is known to increase in wet canopy conditions due to advective effects that are not considered in the Hargreaves model (Hargreaves and Samani, 1985). Without knowing precisely how much  $E_p$  increases due to wet canopy conditions, it is difficult to justify further decreasing  $E_p$  by subtracting interception volumes from it (Calder, 2003). We set  $\Delta_f = 4\text{mm}$  at the forested Elder Creek site (Pypker et al., 2005), and  $\Delta_g = 1\text{mm}$  at the oak savanna Dry Creek site (Feng et al., 2017). The Elder Creek threshold results in an overall rate of interception equal to 16%, which compares well with a value of 13% previously used for the Elder Creek region (Miralles et al., 2010; Salve et al., 2012). At Dry Creek, we calculate 4% of rainfall is lost to interception. This value falls at the lower end of reported values for savannas and dry woodlands (4-10%; Pereira et al., 2009; David et al., 2006), which is to be expected given the Mediterranean-type rainfall regime (relatively infrequent, large storms) and high annual rainfall totals.

## 2.2.6 | Tracking $S_d$ and $S_i$

Direct and indirect storages are tracked at the daily time-step for each year from October 2008 to May 2016 at the Elder Creek site, and from October 2016 to May 2017 in the Dry Creek site. Storages were not tracked for the 2016-2017 water year at Elder Creek because we found that beginning January 2017, USGS discharge measurements were between 0.3 and 0.6  $\text{m}^3/\text{s}$  (at a discharge of 1.9  $\text{m}^3/\text{s}$ ) greater than the presently-used rating curve. This relatively large error in the USGS rating curve could lead to a significant underestimation of catchment discharge and a corresponding overestimation of indirect storage. For example, an underestimate of discharge equal to 0.3  $\text{m}^3/\text{s}$  taken from December through March in the Elder Creek catchment would result in an overestimation of indirect catchment storage equal to approximately 180 mm. This issue highlights the more general drawback that the method requires integration of catchment fluxes over the course of months. Even small errors in daily fluxes could lead to the accumulation of large error.

We also chose to track storages at the daily time-step due to potential transient effects during storm events which would lead to an overestimation of indirect storage. For instance, at Elder Creek, if a large volume of rainfall enters the catchment, it will take a finite time (typically less than a day (Rempe, 2016)) to transit the thick unsaturated zone before reaching the water table that drives discharge (thus registering as direct storage). In this example, the method would temporarily attribute that transient storage to indirect storage. Because we seek to use indirect storage to quantify the hydraulically decoupled storage volumes in the catchment, we average fluxes to the daily time-step as a simple way to avoid such transient effects.

We assume that total catchment storage at the end of the summer (October 1,  $t = 0$ ) is effectively at its minimum achievable value ( $S(0) = S_{min}$  and  $S_d(0) = S_i(0) = 0$ ). We acknowledge that this assumption neglects inter-annual transfers in water storage, but suggest that this simplification is justifiable in Mediterranean climates where total storage at the end of the summer dry season may be considered close to its minimum value. Identifying the timing of a minimum storage state in other climates may be more difficult, but would not preclude application of the method.

From the Oct. 1 initial condition, we numerically integrate Equations 6 and 7 using the computed expression for  $g(Q)$  and the trapezoidal rule to obtain an annual time series for  $S_i$  and  $S_d$ . In order to avoid potentially negative values of  $S_i$  at the start of the water year before any rain has fallen, we set  $E_p = 0$  whenever  $S_i = 0$ .

The details of all computational procedures, as well as the data for this study, can be found in supplementary Jupyter notebooks ([http://www.github.com/daviddralle/indirect\\_storage](http://www.github.com/daviddralle/indirect_storage)), in which we implement the above procedures in the Python coding language.

## 3 | RESULTS

### 3.1 | Patterns of direct and indirect storage

Water year time series of indirect ( $S_i$ ) and direct ( $S_d$ ) storages for Elder Creek (2016) and Dry Creek (2017) are plotted in Figure 6. At Elder Creek, the first rains of the water year rapidly increase the volume of indirect storage, which holds at the same order magnitude ( $10^2$  mm) throughout the wet season. The relative stability of indirect storage at Elder Creek is also observed between years, as demonstrated by Figure 7, which plots the annual mean daily maximum of indirect storage at Elder Creek. The maximum is fairly consistent from year to year, with a coefficient of variation equal to 0.18.

Patterns of direct storage at Elder Creek differ from indirect storage in several notable ways. Direct storage is relatively insensitive to the first rains of the wet season, but increases rapidly once indirect storage begins to plateau. While indirect storage increases become less pronounced with additional wet season rainfall, direct storage remains highly sensitive, often varying over two orders of magnitude in the days leading up to and following a rainfall event. For example, in Figure 6, the coefficient of variation of indirect storage from January through March is equal to 0.06, while the coefficient of variation of direct storage is equal to 0.51, indicating that direct storage exhibits nearly an order of magnitude more relative variation than indirect storage. Volumes of indirect storage greatly exceed those of direct storage, meaning that at any given time the majority of catchment water storage that is dynamic on seasonal timescales is not directly coupled to the stream. Over the same months of January through March 2016, Elder Creek indirect storage is calculated to average 400 mm, while direct storage averages 78 mm.

Only one year of data is available for Dry Creek, but over that period patterns of direct and indirect storage are qualitatively similar to those at Elder Creek (Figure 6). At the beginning of the water year, indirect storage rapidly increases to near its seasonal maximum, at which point direct storage begins to respond, remaining highly variable for the rest of the wet season. Like Elder Creek, Dry Creek indirect storage is also observed to be less variable and larger than direct storage, although this does not hold into the spring growing season (March) when indirect storage volumes begin to drop rapidly. These losses are likely an artifact attributable to either slight overestimation of discharge in the rating curve (which would lead to progressive decreases in indirect storage), or the assumption that  $ET = E_p$  in Equation 7, which could overestimate plant water use in February and March, as annual grasses do not reach peak greenness until April or May (Hahm et al., 2017a).

Quantitatively, there are distinct differences between storages at Elder Creek and Dry Creek. At Dry Creek, indirect storage is nearly always less than 200 mm, with a mean winter value (December 2016 - February 2017) equal to approximately 90 mm. Similarly, mean direct storage at Dry Creek in Figure 6 over the winter months equals 12 mm. Whereas reservoir sizes at Elder Creek are larger, measures of variability in storage are larger at Dry Creek, but only for direct storage. The winter coefficient of variation of direct storage is 1.5 at Dry Creek and 0.8 at Elder Creek, whereas the winter coefficient of variation of indirect storage is approximately equal to 0.5 at both sites.

## 4 | DISCUSSION

### 4.1 | Physical identification of indirect storage

To evaluate the method's performance, we rely on hillslope observations of unsaturated and saturated moisture dynamics at the Elder Creek and Dry Creek sites.

#### Elder Creek

At Elder Creek, we hypothesize that indirect storage volumes should approximate hydraulically decoupled, seasonally dynamic unsaturated water storage, while direct storage represents storage in the seasonal water table that drives discharge generation at the channel-hillslope boundary (Rempe, 2016). To test this, we use results from Rempe (2016), who estimates critical zone unsaturated water storage capacity using time-domain reflectometry (TDR) and neutron probe measurements of moisture dynamics along the Rivendell hillslope. TDR data track dynamic moisture changes within near-surface soil and saprolite (< 2m), while down-well (see well locations in Figure 3) neutron probe measurements estimate moisture changes in the deeper saprolite and weathered rock (rock moisture, sensu Salve et al., 2012). TDR data show that maximum shallow weathered bedrock and soil moisture storage potential ranges from 30 mm to 130 mm, with no systematic variation across the hillslope (Salve et al., 2012; Rempe, 2016). Rock moisture storage generally increases moving upslope toward the divide (away from Elder Creek), consistent with the thickening of the weathered zone (Rempe and Dietrich, 2014), reaching a calculated maximum of 615 mm at the ridge well 15 (see site map in Figure 3). Averaged over the Rivendell hillslope, Rempe (2016) estimate total rock moisture storage capacity to equal 284 mm. Assuming soil moisture storage capacity is equal to the mean of the observed range (80 mm), this leads to maximum unsaturated water storage capacity equal to 364. This measured water storage capacity falls within the estimated range of maximum indirect storage capacity –  $380 \pm 60$  mm (Figure 7). Slight overestimation by indirect storage is expected, as the indirect storage maxima are chosen from daily samples over the course of all wet seasons, while actual measurements of unsaturated moisture volumes are comparably sparse due to the time commitment required to use the neutron probe (Rempe, 2016). We conclude that inferred volumes of indirect storage are consistent with measured estimates of total unsaturated water storage in the Elder Creek catchment.

#### Dry Creek

Validating indirect storage estimates at Dry Creek is more difficult due to the fact that water tables frequently reach the ground surface in areas underlain by predominantly mélange matrix, eliminating the vadose zone. Therefore, we rely on well response data to place bounds on the possible range of indirect water storage during the winter months.

At the start of the wet season, while the stream remains dry and before water tables begin to respond to the first storms, dynamic water storage in the catchment is unsaturated, and – by definition, because there is no discharge – indirect. Once water tables approach the surface, any inferred indirect storage must be saturated. Throughout the winter months, the Dry Creek watershed lies somewhere between these two scenarios. Therefore, cumulative rainfall to the first well response of the wet season places a lower bound on indirect storage volumes (after initial wetting, and before significant water use in the spring), and cumulative rainfall to initial complete saturation of the critical zone places an upper bound on the possible volume of indirect storage in the catchment. Figure 8 (adapted from Hahm et al. (2017a)) shows Tukey boxplots for the range of cumulative rainfall to first response and complete saturation across the collection of wells at the Dry Creek site (mapped in Figure 4). Taking median values (the center line of the boxplots) across the wells as representative, we estimate that hydraulically decoupled storage at Dry Creek should range between a lower bound of 90 mm and an upper bound of 160 mm after the initial wet-up. These bounds are consistent with

inferred indirect storage volumes at Dry Creek; the maximum value is equal to 180 mm, and the mean winter indirect storage (plus or minus one standard deviation) is equal to  $90 \pm 45$  mm.

At Dry Creek in water year 2017, water tables rose to the ground surface and receded repeatedly throughout October and November, while indirect storage volumes remained relatively stable. This suggests that indirect storage at Dry Creek occurs as a time-varying combination of unsaturated and saturated storage. To make a case for this argument, we use well data and observations of CZ structure observed in boreholes. At the beginning of the wet season, Figure 8 shows that a median of 90 mm of water falls on the landscape before the first response in wells with shallow groundwater (2 - 3 m from the surface). During this initial wet-up period (Figure 9, interval 1), wells have not responded and little or no discharge occurs in the stream, hence, total dynamic catchment storage is interpreted to be entirely unsaturated, indirect storage. Between the first rains and the time when all water tables in wells drilled into primarily mélange matrix first reach the ground surface (interval 2), indirect storage increases to plateau at a maximum value approximately equal to 180 mm. At the point when all wells have reached the surface (approximately 200 mm of cumulative rainfall, the start of interval 3), all the indirect storage in the mélange matrix must be saturated storage. Following the rainy period at the start of interval 3, well levels again drop during a rainless period, despite the fact that indirect storage remains roughly constant.

The finding that indirect storage potentially occurs as saturated storage differentiates Dry Creek from Elder Creek, where unsaturated soil and rock moisture account for indirect storage volumes. We hypothesize that saturated, indirect storage in the mélange can occur throughout the catchment in one of three ways:

1. In this thin critical zone, saturated, indirect storage may be retained in the low conductivity weathered melange matrix below the more conductive near surface layers and progressively depleted by evapotranspiration. Hydraulic conductivity profiles from Guelph permeameter measurements (Figure 10) exhibit a consistently large drop between 30 and 60 cm below the surface, suggesting that deeper water stores may not be able to drain efficiently on seasonal timescales. Storage in this non-conductive material could remain dynamic due to primarily evaporative water losses made possible by a thin CZ. Well recession data supports this mechanism; over a month after streams have dried and the herbaceous annual groundcover has senesced, some wells continue to lower through the summer dry season (Figure 11).
2. Irregular subsurface topography of low conductivity bedrock could lead to lateral, hydraulic disconnection of saturated storage from streams. This hypothesis is supported by numerous lines of evidence. Water table elevations in adjacent wells can remain meters apart over the course of the year and during extended dry periods. For example, wells 506 and 507 are located approximately 2 m apart horizontally and at identical elevations (Figure 4), yet water table positions in the two wells differ by nearly 2 m throughout the dry season (Figure 11). This finding suggests potential lateral hydraulic disconnection over very short distances. The rapid drop of groundwater tables in early wet season rain storms without significant discharge generation indicates lateral redistribution of saturated water that is nevertheless disconnected from the stream or neighboring wells. End-of-summer well recession data indicate that perennially-saturated material occurs at varying depths. Again referencing wells 506 and 507 in Figure 11, water table depths recede only until September, at which point water table positions are constant while maintaining a nearly 2 m difference in elevations for over a month. Material samples collected during borehole drilling also suggest that the depth to unweathered, effectively impermeable material can vary over the landscape as a result of the chaotic block-in-matrix fabric of the mélange. For example, in drilling the borehole for well 501 we encountered highly heterogeneous material: loose, grey-brown granular soil-like material and mélange matrix between 0 m and 4.5 m, unweathered mélange matrix from 4.5 to around 6 m, to hard crystalline material between 6 m and 9 m, and then back to mélange matrix beyond 9 m. In comparison, hand auguring in well 8 at the end of

summer 2015 revealed saturated mélange matrix at a depth of 2 m. This degree of vertical variability in bedrock material properties is common across the site, and can also arise due to both the chaotic distribution of blocks within the mélange matrix and the pervasive occurrence of earthflows with listric or undulating basal shear surfaces (Roering et al., 2009; Lee et al., 2017). The resulting undulating low-hydraulic conductivity surface(s) along the relatively low relief, hummocky hillslopes in the mélange (the mean hillslope gradient at Dry Creek is 27.9%, compared to over 50% at Elder Creek) may trap significant volumes of saturated water that leave the catchment via ET.

3. The volume of indirect storage may equal the immobile water volume in a saturated, mobile-immobile matrix. Classic mobile-immobile theory divides complex media (here, the mélange matrix) into two domains differentiated by their respective representations of the physics of water transport (Koch and Flühler, 1993). In the mobile domain, water transport is commonly described by an advection-diffusion equation, whereas transport in the immobile domain is purely diffusive. Support for the mobile-immobile hypothesis relies on the observation that Dry Creek indirect storage remains nearly constant as water tables rise to intersect the ground surface, and subsequently recede (Figure 8, intervals 2 and 3). This suggests that indirect storage may occur as the constant volume of non-draining storage held below an effective 'field capacity' in the mélange matrix, whereas direct storage is the freely draining mobile fraction above 'field capacity'. Hydraulic groundwater models account for these effects with a 'drainable porosity' or 'specific yield' parameter, recognizing that residual pore water remains stored under tension in unsaturated media as a water table recedes (e.g. Hilberts et al., 2005). We stress that this hypothesis does not imply a separation between immobile and mobile pools; only that the volume of the immobile pool is not increasing or decreasing as the water table rises and recedes.

#### 4.1.1 | Reconciling hillslope observations with lumped, catchment-scale quantities

A unique feature of this study is that hillslope measurements of storage dynamics are used to validate and interpret volumes of direct and indirect storage calculated at catchment scales. At two sites with contrasting CZ structure, we showed that the method provides reasonable estimates of hydraulically decoupled storage volumes. This is promising evidence that the method could be used to estimate indirect storage across a range of catchments with different physiographic characteristics. Although the patterns of direct and indirect storage between the two sites are qualitatively similar, these terms nonetheless correspond to very different combinations of saturated and unsaturated water storage. In Elder Creek, the maximum magnitude of indirect storage is relatively constant from year to year (Figure 7), and consistent with the measured range of unsaturated moisture storage inferred from near surface TDR and deep neutron probe profiles. The thick CZ at Elder Creek provides a distinct physical separation between a dynamic unsaturated zone and a hillslope groundwater table, which leads to the relatively straightforward interpretation of indirect storage at Elder Creek as vadose zone storage. In the Dry Creek catchment, there is not necessarily such a separation. At many points throughout the wet season, water tables intersect the ground surface and the catchment effectively has no vadose zone. Bulk water content in much of the critical zone flips back and forth between unsaturated and saturated with each large winter storm.

Our observations indicate that CZ structure controls both the physical position of indirect storage relative to direct storage, as well as the energetic state (saturated or unsaturated) of the storages. At Elder Creek, indirect storage occurs primarily as unsaturated moisture above the direct storage situated deeper in hillslope aquifers. In contrast, Dry Creek indirect storage is interpreted to occur throughout the CZ profile as unsaturated moisture in the early wet season when rains wet but do not saturate near surface soils, saprolite, and weathered bedrock. After the first significant storm of the wet season, water tables rise to the surface and direct storage generates discharge as shallow subsurface stormflow and

overland flow. At this point, direct storage may lie above indirect storage, which occurs as deeper saturated moisture that is hydraulically decoupled from the stream; or, the physical domains of direct and indirect storage may overlap in a saturated, mobile-immobile matrix, where the volume of direct storage equals the volume of freely draining mobile water, and indirect storage the immobile volume. In the case of the latter, we stress that the methods presented here would not provide information on the exchange of water molecules between mobile and immobile domains, which may occur even while the indirect (or immobile) volume remains constant.

Given the distinctive roles of direct and indirect storage in the process of discharge generation, their physical arrangement and respective energetic statuses may have implications for hydraulic transport and hydrological model formulation. For example, at Elder Creek, Kim et al. (2017) show that chemostasis in the stream can be partially explained by large volumes of tension held unsaturated moisture in soil and weathered rock, which is physically positioned above hillslope groundwater tables, buffering incoming rains and draining chemically reacted waters to the saturated zone during recharge events. In contrast, Dry Creek exhibits relatively greater dilution of major cations at high flows, consistent with shorter residence times and lower fluid-solid interactions during high runoff events dominated by shallow subsurface and saturation overland flow (Hahm et al., 2017c).

Physical positioning of direct and indirect storage also raises the question of appropriate representation of storage dynamics in conceptual hydrologic models. The Elder Creek interpretation aligns with common perceptual understanding of catchment runoff generation: Unsaturated and saturated moisture dynamics can be treated separately (e.g. Botter et al., 2009; Bárdossy and Singh, 2008; Fovet et al., 2015) due to a distinct hydrologic zonation between the dynamic unsaturated zone and hillslope water tables. Interpretation of discharge generation and direct/indirect storage dynamics at Dry Creek, however, presents a more significant challenge for the conceptual hydrologic modeler. Few process-oriented, lumped ecohydrologic modeling frameworks account for a dynamic boundary between saturated and unsaturated moisture layers (e.g. Seibert et al., 2003; Liang et al., 2017).

Between-site variations in the position and energetic status of indirect and direct storages necessitate cautious interpretation of storage metrics for catchment inter-comparison (Buttle, 2016; McNamara et al., 2011). While both Dry Creek and Elder Creek present qualitatively similar storage behaviors, their disparate physical origins challenge unique identification of catchment function from a single index (beyond numerical uncertainty in the computed value of a given metric; e.g. Westerberg and McMillan, 2015). Continued development of catchment scale storage-discharge methods, such as the method presented in this study, and identification of new ‘hydrological signatures’ of critical zone structure (Thompson et al., 2015) could help to increase the power of comparative hydrologic methods (Staudinger et al., 2017)

#### 4.1.2 | Storage metrics for estimating critical zone properties

Despite challenges relating to its precise physical interpretation, indirect storage may still be useful for understanding hydrological partitioning in the critical zone, especially relating to recent efforts to estimate ‘plant available water storage capacity’ of the subsurface (Brooks et al., 2011; Garcia and Tague, 2015). Under the assumption that significant transfers of water from indirect to direct storage are negligible 24 hours after rainfall (notably, similar assumptions are implicit in studies that use the methods from Kirchner (2009) to estimate dynamic storage volumes), the only way that indirect storage can decrease between rainfall events is through evapotranspiration. This is evident from the box diagram in Figure 1 when  $R \approx 0$ . While vegetation may use direct storage, we showed that indirect storage volumes are significantly larger than direct storage volumes, even in catchments with radically disparate CZ structure (tenfold difference in the thickness of the subsurface weathered zone). Furthermore, at both sites, the depletion of dynamic water storage during the summer growing season is almost entirely driven by ET; there is little to no summer discharge

in Dry Creek, and an average of 35 mm of discharge from June to August in Elder Creek. Therefore, indirect storage maxima may provide a reasonable lower bound on the plant available water storage capacity of catchments.

Quantifying the volume of catchment storage that is available for vegetation water use is important for explaining extant biogeographical patterns (Hahm et al., 2017a), predicting ET response to climate change (Garcia and Tague, 2015), improving hydrologic representation of the subsurface in earth system models (Lawrence et al., 2011; Brunke et al., 2016), and understanding vegetation water stress (Porporato et al., 2004). The benefit of the presented approach is that it does not require extensive data for model calibration; it is largely an empirical approach relying solely on catchment scale fluxes, meaning that it could be used to obtain a first approximation of plant available water storage capacity in less intensively monitored catchments.

## 5 | CONCLUSION

The fundamental premise of this study is that seasonally dynamic catchment water storage can be partitioned between two distinct pools of water: dynamic direct storage ( $S_d$ ) and dynamic indirect storage ( $S_i$ ). Direct storage is the subsurface dynamic storage that is hydraulically coupled to the stream; knowledge of the magnitude of direct storage is both necessary and sufficient to determine catchment discharge by way of a storage discharge relationship,  $Q = f(S_d)$ . Indirect storage, on the other hand, is the volume of water that is dynamic on seasonal timescales yet is not directly hydraulically coupled to the stream. Indirect storage is interpreted as the subsurface storage that is primarily responsible for non-uniqueness or hysteresis in the relationship between total dynamic catchment storage and discharge; it may change in volume without directly impacting rates of stream discharge.

Here we derive an objective procedure for partitioning total wet season dynamic storage into volumes of direct and indirect storage. Using subsurface observations of critical zone moisture dynamics at two intensively monitored sites with radically different critical zone structures and dominant runoff generation mechanisms, we find the method accurately predicts volumes of subsurface water that are not hydraulically coupled to the stream, that is, indirect storage. Surprisingly, indirect storage accounts for most dynamic storage, despite discharge being driven by groundwater or saturation overland flow. In the deep critical zone of the Elder Creek catchment, indirect storage was mostly held as rock moisture in the weathered bedrock, and to a lesser extent as near-surface soil moisture. In the shallow critical zone of the Dry Creek catchment, indirect storage was held as soil and rock moisture, but also as saturated (groundwater) storage that did not drain laterally to streams. Good model performance between our two study watersheds, which have large differences in critical zone thickness and hydrology, suggests the model may be applicable to physiographically diverse catchments, and warrants further evaluation at novel sites.

## ACKNOWLEDGEMENTS

N.J.K. was supported by the Babson Faculty Research Fund. W.J.H. was supported by the Mildred E. Mathias Graduate Student Research Grant. All authors acknowledge support from the National Science Foundation CZP EAR-1331940 for the Eel River Critical Zone Observatory. LiDAR data was funded through The National Center for Airborne Laser Mapping (<http://ncalm.cive.uh.edu/>), and is available at OpenTopography (<http://www.opentopography.org/>). Data and the analyses presented in this study can be obtained through GitHub at [http://www.github.com/daviddralle/indirect\\_storage](http://www.github.com/daviddralle/indirect_storage).

## REFERENCES

- Allen, R. G., Pereira, L. S., Raes, D., Smith, M. et al. (1998) Crop evapotranspiration-guidelines for computing crop water requirements-fao irrigation and drainage paper 56. FAO, Rome, 300.
- Bárdossy, A. and Singh, S. K. (2008) Robust estimation of hydrological model parameters. *Hydrology and Earth System Sciences*, **12**, 1273–1283. URL: <https://doi.org/10.5194/hess-12-1273-2008>.
- Beven, K. (1989) Changing ideas in hydrology – the case of physically-based models. *Journal of Hydrology*, **105**, 157–172.
- Birkel, C., Soulsby, C. and Tetzlaff, D. (2011) Modelling catchment-scale water storage dynamics: reconciling dynamic storage with tracer-inferred passive storage. *Hydrological Processes*, **25**, 3924–3936.
- Blake Jr., M. C. and Jones, D. L. (1974) Origin of franciscan melanges in northern california. *19*, 345–357.
- Botter, G., Porporato, A., Rodriguez-Iturbe, I. and Rinaldo, A. (2007) Basin-scale soil moisture dynamics and the probabilistic characterization of carrier hydrologic flows: Slow, leaching-prone components of the hydrologic response. *Water Resources Research*, **43**.
- (2009) Nonlinear storage-discharge relations and catchment streamflow regimes. *Water resources research*, **45**.
- Brauer, C. C., Teuling, A. J., Torfs, P. J. J. F. and Uijlenhoet, R. (2013) Investigating storage-discharge relations in a lowland catchment using hydrograph fitting, recession analysis, and soil moisture data. *Water Resources Research*, **49**, 4257–4264. URL: <https://doi.org/10.1002/wrcr.20320>.
- Brooks, P. D., Troch, P. A., Durcik, M., Gallo, E. and Schlegel, M. (2011) Quantifying regional scale ecosystem response to changes in precipitation: Not all rain is created equal. *Water Resources Research*, **47**.
- Brunke, M. A., Broxton, P., Pelletier, J., Gochis, D., Hazenberg, P., Lawrence, D. M., Leung, L. R., Niu, G.-Y., Troch, P. A. and Zeng, X. (2016) Implementing and evaluating variable soil thickness in the community land model, version 4.5 (CLM4.5). *Journal of Climate*, **29**, 3441–3461.
- Brutsaert, W. and Nieber, J. L. (1977) Regionalized drought flow hydrographs from a mature glaciated plateau. *Water Resources Research*, **13**, 637–643.
- Buttle, J. M. (2016) Dynamic storage: a potential metric of inter-basin differences in storage properties. *Hydrological Processes*, **30**, 4644–4653.
- Calder, I. R. (2003) Assessing the water use of short vegetation and forests: Development of the hydrological land use change (HYLUC) model. *Water Resources Research*, **39**.
- Cloos, M. (1983) Comparative study of melange matrix and metashales from the franciscan subduction complex with the basal great valley sequence, california. *The Journal of Geology*, **91**, 291–306.
- Coutagne, A. (1948) Les variations de débit en période non influencée par les précipitations-le débit d'infiltration (corrélations fluviales internes) 2ème partie. *La Houille Blanche*, 416–436.
- Creutzfeldt, B., Troch, P. A., Güntner, A., Ferré, T. P. A., Graeff, T. and Merz, B. (2013) Storage-discharge relationships at different catchment scales based on local high-precision gravimetry. *Hydrological Processes*, **28**, 1465–1475.
- David, T. S., Gash, J. H. C., Valente, F., Pereira, J. S., Ferreira, M. I. and David, J. S. (2006) Rainfall interception by an isolated evergreen oak tree in a mediterranean savannah. *Hydrological Processes*, **20**, 2713–2726.
- Dupuit, J. É. J. (1863) *Études théoriques et pratiques sur le mouvement des eaux dans les canaux découverts et à travers les terrains perméables: avec des considérations relatives au régime des grandes eaux, au débouché à leur donner, et à la marche des alluvions dans les rivières à fond mobile*. Dunod, Paris.

- Elrick, D. E. and Reynolds, W. D. (1992) Methods for analyzing constant-head well permeameter data. *Soil Science Society of America Journal*, **56**, 320.
- Feng, X., Dawson, T. E., Ackerly, D. D., Santiago, L. S. and Thompson, S. E. (2017) Reconciling seasonal hydraulic risk and plant water use through probabilistic soil-plant dynamics. *Global Change Biology*, **23**, 3758–3769.
- Fovet, O., Ruiz, L., Hrachowitz, M., Faucheuix, M. and Gascuel-Odoux, C. (2015) Hydrological hysteresis and its value for assessing process consistency in catchment conceptual models. *Hydrology and Earth System Sciences*, **19**, 105–123.
- Garcia, E. S. and Tague, C. L. (2015) Subsurface storage capacity influences climate–evapotranspiration interactions in three western united states catchments. *Hydrology and Earth System Sciences*, **19**, 4845–4858.
- Grant, G. E. and Dietrich, W. E. (2017) The frontier beneath our feet. *Water Resources Research*, **53**, 2605–2609.
- Hahm, W. J., Dawson, T. E. and Dietrich, W. E. (submitted) Controls on the distribution and resilience of *q. garryana*: ecophysiological evidence of oak water-limitation tolerance. *Ecological Monographs*.
- Hahm, W. J., Dietrich, W. E., Rempe, D. M., Dralle, D. N., Dawson, T. E., Lovill, S. and Bryk, A. (2017a) The influence of critical zone structure on runoff paths, seasonal water storage, and ecosystem composition. In *AGU Fall Meeting Conference Abstracts*.
- Hahm, W. J., Dralle, D. N., Lovill, S. M., Rose, J., Dawson, T. and Dietrich, W. E. (2017b) Exploratory tree survey (2016 - eel river critical zone observatory - sagehorn - central belt melange, franciscan complex, northern california coast ranges, usa). *Hydroshare*.
- Hahm, W. J., Wang, J., Druhan, J. L., Rempe, D. M. and Dietrich, W. E. (2017c) Relating runoff generation mechanisms to concentration-discharge relationships in catchments with well-characterized critical zone structures and hydrologic dynamics. In *AGU Fall Meeting Conference Abstracts*.
- Hall, F. R. (1968) Base-flow recessions-a review. *Water Resources Research*, **4**, 973–983.
- Hansen, M. C., Potapov, P. V., Moore, R., Hancher, M., Turubanova, S. A., Tyukavina, A., Thau, D., Stehman, S. V., Goetz, S. J., Loveland, T. R., Kommareddy, A., Egorov, A., Chini, L., Justice, C. O. and Townshend, J. R. G. (2013) High-resolution global maps of 21st-century forest cover change. *Science*, **342**, 850–853.
- Hargreaves, G. H. and Samani, Z. A. (1985) Reference crop evapotranspiration from temperature. *Applied engineering in agriculture*, **1**, 96–99.
- Hilberts, A. G. J., Troch, P. A. and Paniconi, C. (2005) Storage-dependent drainable porosity for complex hillslopes. *Water Resources Research*, **41**.
- Holbrook, W. S., Riebe, C. S., Elwaseif, M., Hayes, J. L., Basler-Reeder, K., Harry, D. L., Malazian, A., Dosseto, A., Hartsough, P. C. and Hopmans, J. W. (2014) Geophysical constraints on deep weathering and water storage potential in the southern sierra critical zone observatory. *Earth Surface Processes and Landforms*, **39**, 366–380.
- Horton, R. E. (1936) Natural stream channel-storage. *Transactions, American Geophysical Union*, **17**, 406.
- Jayko, A. S., Blake, M. C., McLaughlin, R. J., Ohlin, H. N., Ellen, S. D. and Kelsey, H. M. (1989) Reconnaissance Geologic Map of the Covelo 30- by 60-Minute Quadrangle, Northern California. URL: [http://ngmdb.usgs.gov/ProdDesc/proddesc\\_327.htm](http://ngmdb.usgs.gov/ProdDesc/proddesc_327.htm).
- Kim, H., Bishop, J. K., Dietrich, W. E. and Fung, I. Y. (2014) Process dominance shift in solute chemistry as revealed by long-term high-frequency water chemistry observations of groundwater flowing through weathered argillite underlying a steep forested hillslope. *Geochimica et Cosmochimica Acta*, **140**, 1–19.
- Kim, H., Dietrich, W. E., Thurnhoffer, B. M., Bishop, J. K. B. and Fung, I. Y. (2017) Controls on solute concentration-discharge relationships revealed by simultaneous hydrochemistry observations of hillslope runoff and stream flow: The importance of critical zone structure. *Water Resources Research*, **53**, 1424–1443.

- Kirchner, J. W. (2009) Catchments as simple dynamical systems: Catchment characterization, rainfall-runoff modeling, and doing hydrology backward. *Water Resources Research*, **45**.
- Koch, S. and Flühler, H. (1993) Solute transport in aggregated porous media: Comparing model independent and dependent parameter estimation. *Water, Air, and Soil Pollution*, **68**.
- Krier, R., Matgen, P., Goergen, K., Pfister, L., Hoffmann, L., Kirchner, J. W., Uhlenbrook, S. and Savenije, H. H. G. (2012) Inferring catchment precipitation by doing hydrology backward: A test in 24 small and mesoscale catchments in luxembourg. *Water Resources Research*, **48**.
- Laio, F., Porporato, A., Ridolfi, L. and Rodriguez-Iturbe, I. (2001) Plants in water-controlled ecosystems: active role in hydrologic processes and response to water stress: II. probabilistic soil moisture dynamics. *Advances in Water Resources*, **24**, 707–723.
- Lawrence, D. M., Oleson, K. W., Flanner, M. G., Thornton, P. E., Swenson, S. C., Lawrence, P. J., Zeng, X., Yang, Z.-L., Levis, S., Sakaguchi, K., Bonan, G. B. and Slater, A. G. (2011) Parameterization improvements and functional and structural advances in version 4 of the community land model. *Journal of Advances in Modeling Earth Systems*, **3**.
- Lee, S. S., Rempe, D. M., Holbrook, W. S., Schmidt, L., Hahm, W. J. and Dietrich, W. E. (2017) Critical zone structure inferred from multiscale near surface geophysical and hydrological data across hillslopes at the eel river czo. In AGU Fall Meeting Conference Abstracts.
- Lehmann, P., Hinz, C., McGrath, G., van Meerveld, H. J. T. and McDonnell, J. J. (2007) Rainfall threshold for hillslope outflow: an emergent property of flow pathway connectivity. *Hydrology and Earth System Sciences*, **11**, 1047–1063.
- Liang, X., Zhan, H., Zhang, Y.-K. and Schilling, K. (2017) Base flow recession from unsaturated-saturated porous media considering lateral unsaturated discharge and aquifer compressibility. *Water Resources Research*.
- Link, P., Simonin, K., Maness, H., Oshun, J., Dawson, T. and Fung, I. (2014) Species differences in the seasonality of evergreen tree transpiration in a mediterranean climate: Analysis of multiyear, half-hourly sap flow observations. *Water Resources Research*, **50**, 1869–1894.
- Lovill, S., Hahm, W. J. and Dietrich, W. E. (2015) Drainage from the critical zone: lithologic, aspect, and vegetation controls on the spatial extent of wetted channels during the summer dry seasons. In AGU Fall Meeting Conference Abstracts.
- McNamara, J. P., Tetzlaff, D., Bishop, K., Soulsby, C., Seyfried, M., Peters, N. E., Aulenbach, B. T. and Hooper, R. (2011) Storage as a metric of catchment comparison. *Hydrological Processes*, **25**, 3364–3371.
- van Meerveld, H. J. T. and McDonnell, J. J. (2006) Threshold relations in subsurface stormflow: 2. the fill and spill hypothesis. *Water Resources Research*, **42**.
- Miralles, D. G., Gash, J. H., Holmes, T. R. H., de Jeu, R. A. M. and Dolman, A. J. (2010) Global canopy interception from satellite observations. *Journal of Geophysical Research*, **115**.
- Nippgen, F., McGlynn, B. L. and Emanuel, R. E. (2015) The spatial and temporal evolution of contributing areas. *Water Resources Research*, **51**, 4550–4573.
- Nippgen, F., McGlynn, B. L., Emanuel, R. E. and Vose, J. M. (2016) Watershed memory at the coweeta hydrologic laboratory: The effect of past precipitation and storage on hydrologic response. *Water Resources Research*, **52**, 1673–1695.
- Oshun, J., Dietrich, W. E., Dawson, T. E. and Fung, I. (2016) Dynamic, structured heterogeneity of water isotopes inside hillslopes. *Water Resources Research*, **52**, 164–189.
- Palmroth, S., Katul, G. G., Hui, D., McCarthy, H. R., Jackson, R. B. and Oren, R. (2010) Estimation of long-term basin scale evapotranspiration from streamflow time series. *Water Resources Research*, **46**.

- Peel, M. C., Finlayson, B. L. and McMahon, T. A. (2007) Updated world map of the köppen-geiger climate classification. *Hydrology and Earth System Sciences*, **11**, 1633–1644.
- Pereira, F., Gash, J., David, J., David, T., Monteiro, P. and Valente, F. (2009) Modelling interception loss from evergreen oak mediterranean savannas: Application of a tree-based modelling approach. *Agricultural and Forest Meteorology*, **149**, 680–688.
- Porporato, A., Daly, E. and Rodríguez-Iturbe, I. (2004) Soil water balance and ecosystem response to climate change. *The American Naturalist*, **164**, 625–632.
- PRISM (2015) PRISM Climate Group, 30 year precipitation normals (1980-2010). URL: <http://prism.oregonstate.edu>.
- Pypker, T. G., Bond, B. J., Link, T. E., Marks, D. and Unsworth, M. H. (2005) The importance of canopy structure in controlling the interception loss of rainfall: examples from a young and an old-growth douglas-fir forest. *Agricultural and forest Meteorology*, **130**, 113–129.
- Rempe, D. M. (2016) *Controls on critical zone thickness and hydrologic dynamics at the hillslope scale*. Ph.D. thesis, University of California, Berkeley.
- Rempe, D. M. and Dietrich, W. E. (2014) A bottom-up control on fresh-bedrock topography under landscapes. *Proceedings of the National Academy of Sciences*, **111**, 6576–6581.
- Riebe, C. S., Hahm, W. J. and Brantley, S. L. (2016) Controls on deep critical zone architecture: a historical review and four testable hypotheses. *Earth Surface Processes and Landforms*, **42**, 128–156.
- Rieger, J. and Tourian, M. J. (2014) Characterization of runoff-storage relationships by satellite gravimetry and remote sensing. *Water Resources Research*, **50**, 3444–3466.
- Rodríguez-Iturbe, I. and Valdés, J. B. (1979) The geomorphologic structure of hydrologic response. *Water Resources Research*, **15**, 1409–1420.
- Roering, J. J., Stimely, L. L., Mackey, B. H. and Schmidt, D. A. (2009) Using DInSAR, airborne LiDAR, and archival air photos to quantify landsliding and sediment transport. *Geophysical Research Letters*, **36**.
- Rupp, D. E. and Selker, J. S. (2006) Information, artifacts, and noise in dq/dt- q recession analysis. *Advances in water resources*, **29**, 154–160.
- Salve, R., Rempe, D. M. and Dietrich, W. E. (2012) Rain, rock moisture dynamics, and the rapid response of perched groundwater in weathered, fractured argillite underlying a steep hillslope. *Water Resources Research*, **48**.
- Sayama, T., McDonnell, J. J., Dhakal, A. and Sullivan, K. (2011) How much water can a watershed store? *Hydrological Processes*, **25**, 3899–3908.
- Seibert, J., Rodhe, A. and Bishop, K. (2003) Simulating interactions between saturated and unsaturated storage in a conceptual runoff model. *Hydrological Processes*, **17**, 379–390.
- Sloan, W. T. (2000) A physics-based function for modeling transient groundwater discharge at the watershed scale. *Water Resources Research*, **36**, 225–241.
- Spence, C., Guan, X. J., Phillips, R., Hedstrom, N., Granger, R. and Reid, B. (2009) Storage dynamics and streamflow in a catchment with a variable contributing area. *Hydrological Processes*, **24**, 2209–2221.
- Staudinger, M., Stoelze, M., Seeger, S., Seibert, J., Weiler, M. and Stahl, K. (2017) Catchment water storage variation with elevation. *Hydrological Processes*, **31**, 2000–2015.
- Tani, M. (2008) Analysis of runoff-storage relationships to evaluate the runoff-buffering potential of a sloping permeable domain. *Journal of Hydrology*, **360**, 132–146.

- Thompson, S. E., Karst, N. and Dralle, D. (2015) Hydrological signatures of critical zone processes: Developing targets for critical zone modeling. *AGU Fall Meeting Abstracts*.
- Torres, R., Dietrich, W. E., Montgomery, D. R., Anderson, S. P. and Loague, K. (1998) Unsaturated zone processes and the hydrologic response of a steep, unchannelled catchment. *Water Resources Research*, **34**, 1865–1879.
- Westerberg, I. K. and McMillan, H. K. (2015) Uncertainty in hydrological signatures. *Hydrology and Earth System Sciences*, **19**, 3951–3968.
- Yang, D., Goodison, B. E., Ishida, S. and Benson, C. S. (1998) Adjustment of daily precipitation data at 10 climate stations in alaska: Application of world meteorological organization intercomparison results. *Water Resources Research*, **34**, 241–256.

**TABLE 1** Catchment descriptions

	Elder Creek	Dry Creek
<b>Catchment lithology</b>	Coastal Belt: Deep, fractured mudstone and sandstone	Central Belt: Argillite-matrix mélange with suspended blocks of varying lithology
<b>Drainage area (km<sup>2</sup>)</b>	16.9	3.5
<b>Primary vegetation cover</b>	Mixed broadleaf-needleleaf, evergreen forest	Annual grass, deciduous oak savanna
<b>Mean elevation (meters AMSL)</b>	849	733
<b>Mean annual precipitation (mm) 1981-2010, PRISM data (PRISM, 2015)</b>	2042	1811

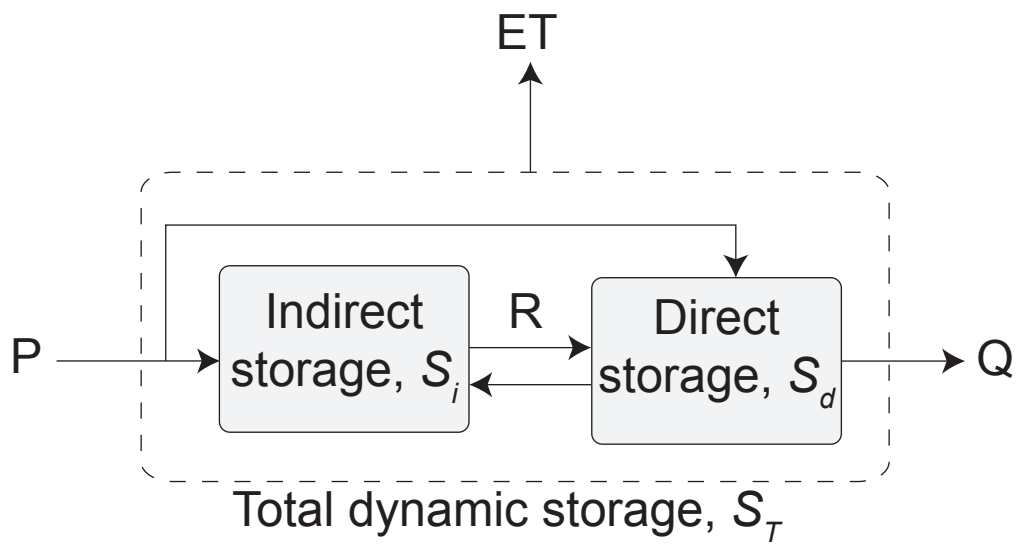


**FIGURE 1** Box diagram illustrating the relationship and fluxes between total dynamic storage, direct storage, and indirect storage.

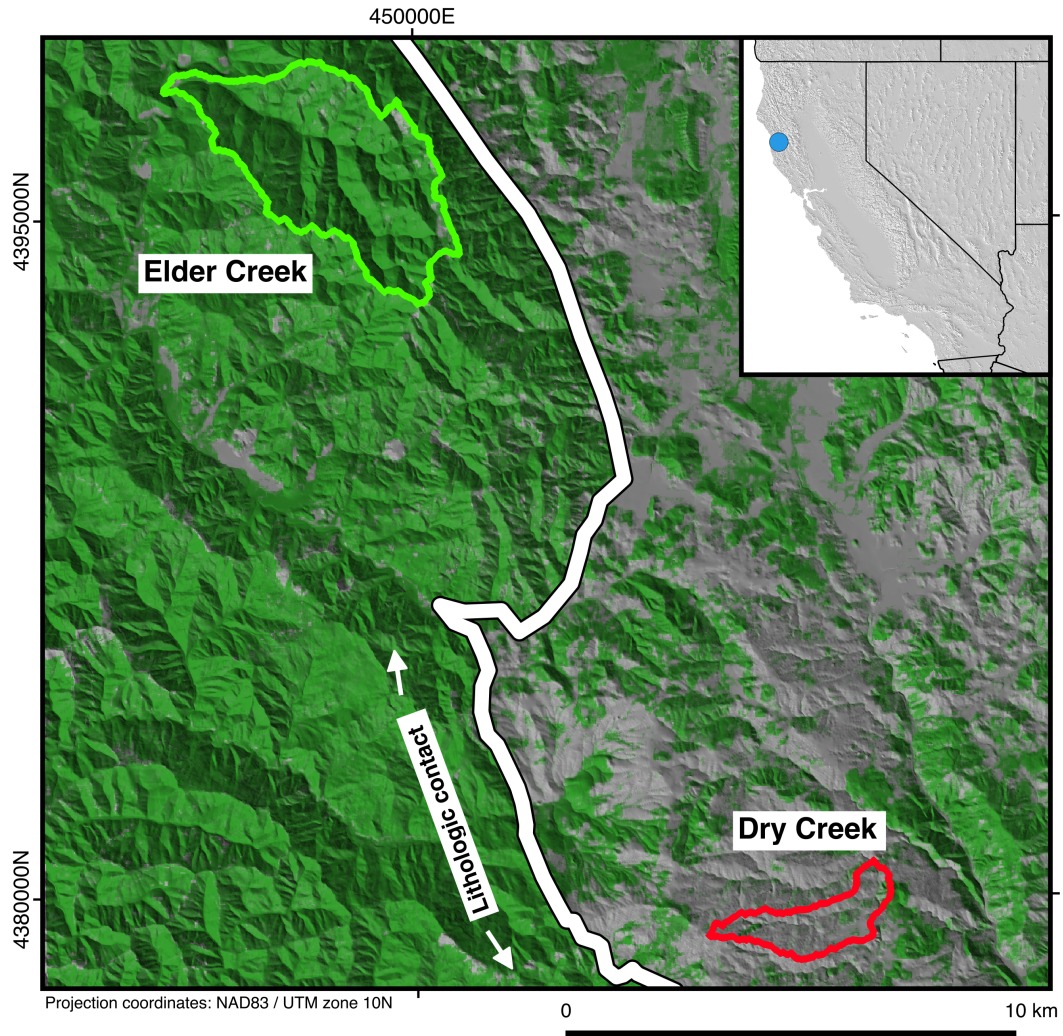


**FIGURE 2** Regional map of the Dry Creek and Elder Creek watersheds. The thick white line plots the lithologic contact (Jayko et al., 1989) between the Coastal Belt (turbidites) to the west and the Central Belt (mélange) to the east. Gray to green pseudo-color represents percent forest cover from 0% to 100%, respectively (Hansen et al., 2013). Inset shows the state of California with a blue point for the study watersheds location.

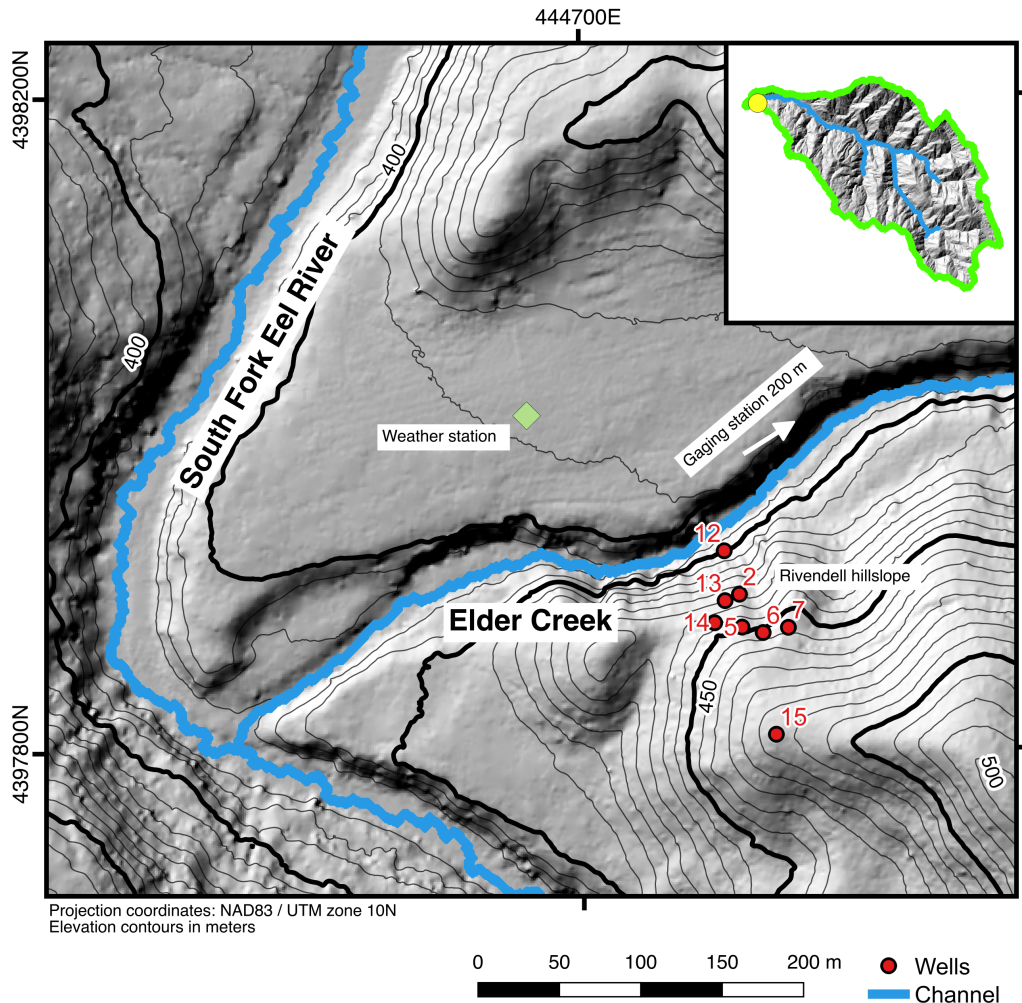


**FIGURE 3** Bare earth hillshade map of the Elder Creek study area generated from 1 m digital elevation model derived from data provided by the National Center for Airborne Laser Mapping. Inset shows the entire Elder Creek watershed, and the yellow point corresponds to the intensive monitoring site (Rivendell). Eight wells are used to record ground water fluctuations and to make repeat neutron probe measurements.

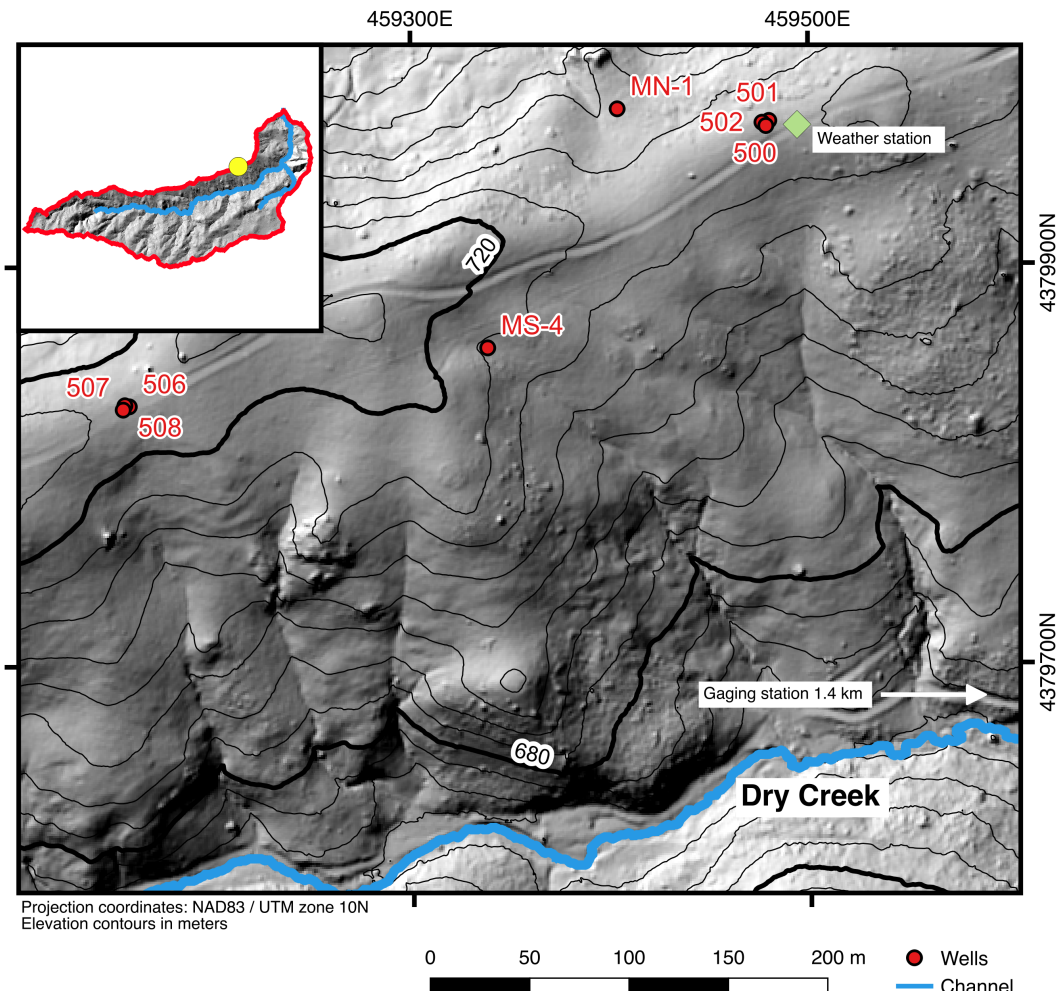


**FIGURE 4** Bare earth hillshade map of the Dry Creek study area generated from 1 m digital elevation model derived from data provided by the National Center for Airborne Laser Mapping. Inset shows the entire Dry Creek watershed, and the yellow point corresponds to the intensive monitoring site. Eight wells are used to record ground water fluctuations and to make repeat neutron probe measurements.

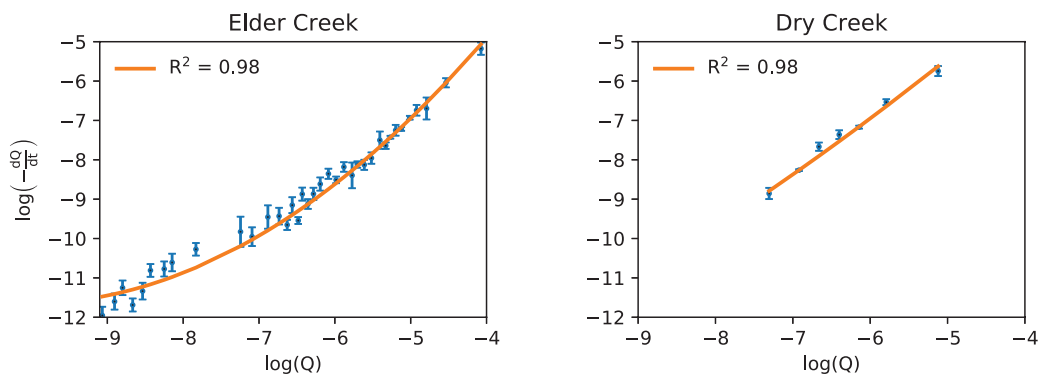


**FIGURE 5** Plots of binned mean values (green dots) of  $\log(-dQ/dt)$  versus corresponding values of  $\log Q$ . The standard error in each bin is represented with whiskers on each point.

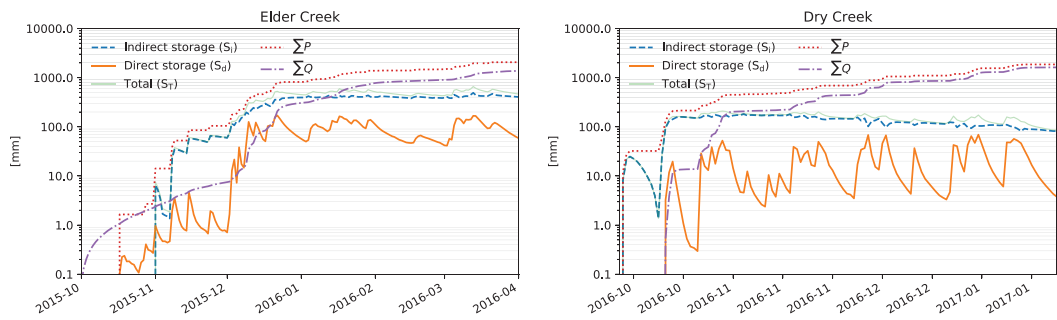


**FIGURE 6** Direct storage ( $S_d$ ), indirect storage ( $S_i$ ), total dynamic storage ( $S_T$ ), cumulative seasonal precipitation ( $\sum P$ ), and cumulative seasonal discharge ( $\sum Q$ ) time series at Elder Creek for the 2015–2016 water year, and at Dry Creek for the 2016–2017 water year.

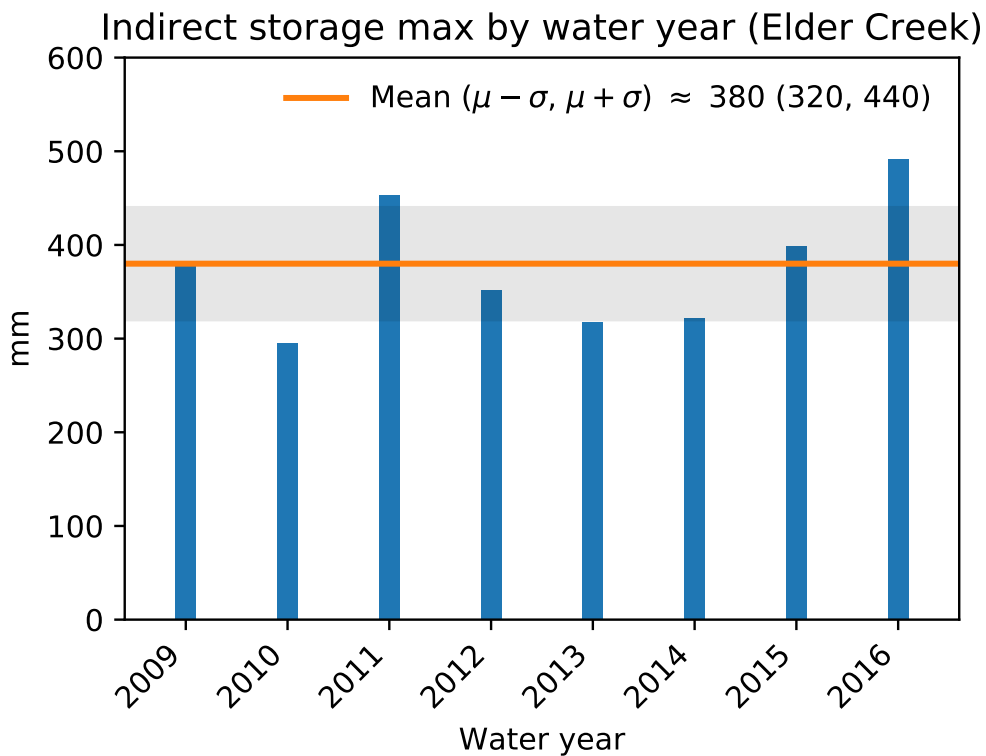


**FIGURE 7** Maximum calculated indirect storage ( $S_i$ ) at Elder Creek (with the grey envelope representing the mean plus or minus one standard deviation) for water years 2009–2016.

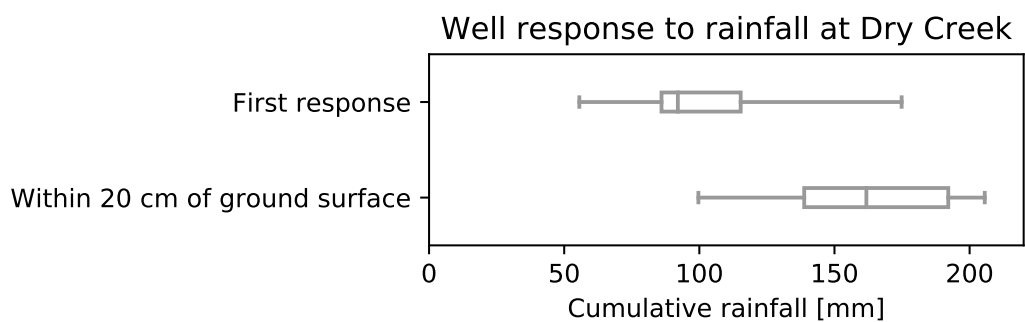


**FIGURE 8** Cumulative rainfall at Dry Creek until the first response (first decrease in depth to water table at the start of the wet season) of well water tables and for each well to rise to within 20 cm of the surface.

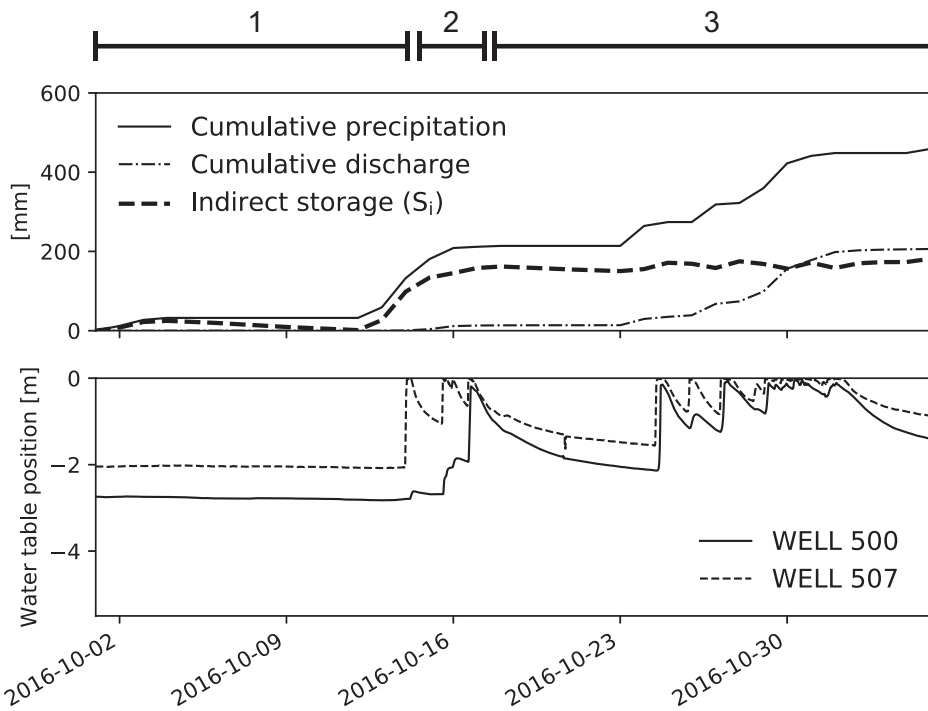


**FIGURE 9** Early wet season dynamics of direct, indirect, and total dynamic storages in Dry Creek (top). Two well time series (bottom) demonstrate variable thresholds for water table response and complete saturation to the ground surface.

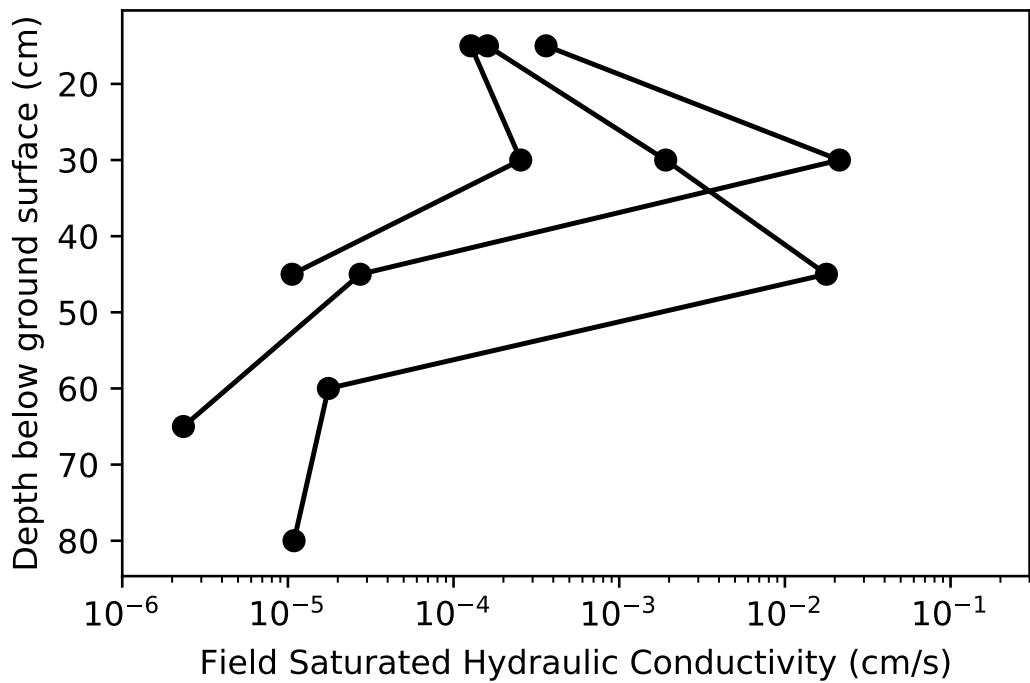


**FIGURE 10** Measurements of saturated hydraulic conductivity with depth adjacent to wells 506 - 508 at Dry Creek.

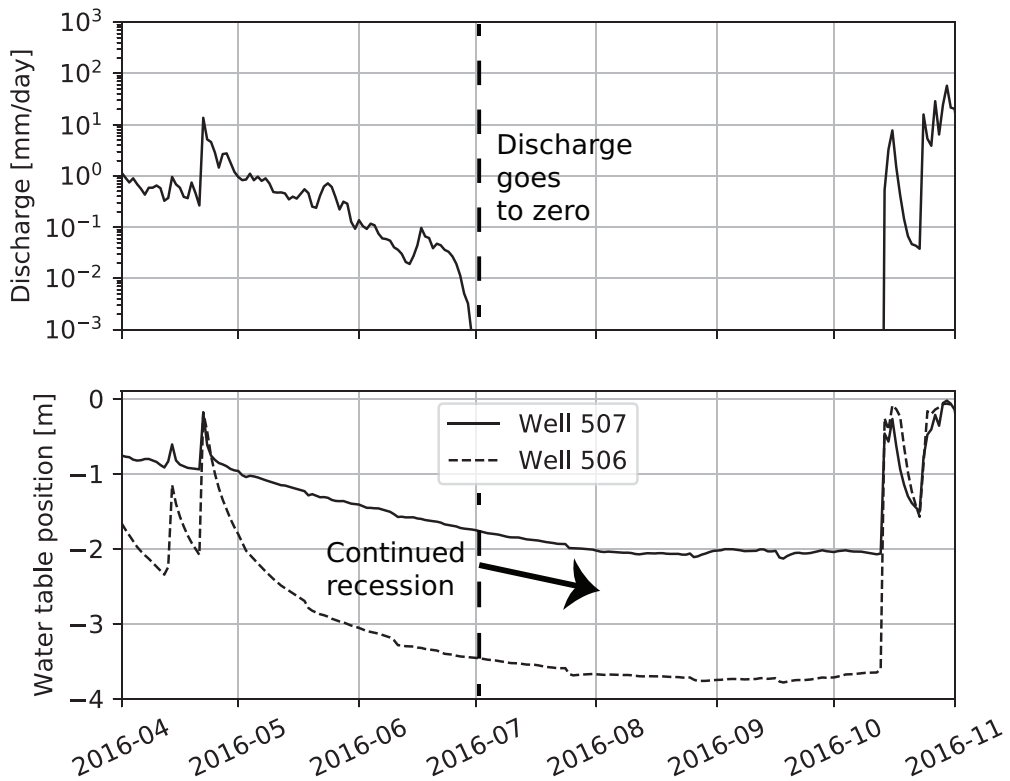


**FIGURE 11** Daily average discharge in Dry Creek and daily average depth to the water table in wells 506 and 507. Despite only two meters of separation between the two wells, nearly two meters separate water table positions throughout the dry season. Well recessions also continue long after stream discharge goes to zero, suggesting that indirect storage may occur in the saturated zone.